Ultrarelativistic electromagnetic pulses in plasmas

M. Ashour-Abdalla, J. N. Leboeuf, T. Tajima, J. M. Dawson, and C. F. Kennel
Department of Physics, University of California, Los Angeles, California 90024
(Received 4 August 1980)

We study through computer simulation the physical processes of a linearly polarized electromagnetic pulse of highly relativistic amplitude ($eE/m\omega c \gg 1$) in an underdense plasma accelerating particles to very high energies. We consider first an electron-positron plasma. The maximum momenta achieved scale as the square of the wave amplitude. This acceleration stops when the bulk of the wave energy is converted to particle energy. The pulse leaves behind as a wake a vacuum region whose length scales as the amplitude of the wave. The results can be explained in terms of a snow plow or pistonlike action of the radiation on the plasma. When a mass ratio other than unity is chosen and electrostatic effects begin to play a role, first the ion energy increases faster than the electron energy and then the electron energy catches up later, eventually reaching the same value.

I. INTRODUCTION

The interaction of intense electromagnetic waves with a plasma has been studied in the context of laser fusion and pulsar astrophysics over the last decade. The advent of the technology of intense lasers as well as the development of the technology of intense microwave sources have spurred a concerted analytical, experimental, and simulation effort. Various studies show that wave-induced plasma nonlinearities lead to enhanced absorption as well as stimulated reflection of radiation.[1] The latest potentially important application of intense irradiation of a plasma is the laser electron accelerator,[2] or more generally speaking, radiation electron accelerator. Here, a relativistic amplitude ($eE/m\omega c \gg 1$) of the electromagnetic wave is needed for efficient acceleration; a relativistic amplitude or wave is defined as a wave whose electron quivering velocity $eE/m\omega$ reaches or exceeds the speed of light, where E and ω are the wave electric field and frequency and e and m are the electronic charge and rest mass.

Earlier, Kaw and Dawson[3] demonstrated that a relativistic wave can propagate in an overdense plasma, because the relativistic electron oscillations in the wave increase the electron transverse mass, and thereby reduce the critical frequency. In an astrophysical context, Max and Perkins[4] considered amplitudes such that the quivering electron velocity greatly exceeds the speed of light (with the ions still nonrelativistic). When the wave energy density greatly exceeds the ion rest mass energy density, electrons and ions behave alike, since their inertia is neglible and the kinetic energy is almost proportional to the momentum for both species.[5] An electron-positron plasma model then may be a convenient one to describe such ultrarelativistic waves.[6] Such high amplitude electromagnetic waves may occur in the outer magnetosphere of pulsars[7] and Sturrock[8] argues that their magnetospheres may be largely positronic plasmas.

The fluid equations for a relativistic plasma do not have a unique way to truncate the velocity moments hierarchy[9] as in the case for a nonrelativistic plasma; it can have a closed form only when the plasma is assumed cold (zero temperature) in the presence of relativistic waves. It is, however, obviously unrealistic to assume this, since such strong waves are expected to cause strong particle-wave interactions. It is thus a formidable task to tackle these problems by a fluid theory. The integration of the relativistic Vlasov equation is also quite difficult because of the nonlinear nature of the Lorentz force term, among others. It appears that a computer simulation provides a powerful, and perhaps the only fully available tool to investigate such problems, since experiments at this point are beyond technical possibility, and for such things as pulsar fields ($B = 10^{12}$ G) will remain so. Our computer model, described in detail in the next section, is a fully self-consistent relativistic electromagnetic particle code which allows three-directional electric- and magnetic-field components and three-directional velocities, but only one-directional spatial variation (one- and two-halves-dimensional code).

The present paper focuses on cases with ultrarelativistic electromagnetic pulses in an underdense plasma. The waves are so relativistic that we use the electron-positron model in most cases. A study of cases with mass ratio different from unity is then presented. The interaction is examined as an initial value problem in the kinetic description of the simulation. The electric and magnetic fields are chosen to correspond to an initially linearly polarized localized pulse. The particle momenta in the pulse region of space are self-consistently perturbed *ab initio* over their background Maxwellian velocity distribution arrangement. The frequencies chosen are well above the plasma fre-

quency. The following are physical phenomena that characterize the interaction. Large local energy deposition by the relativistic pulse and the ponderomotive force expels the plasma from a region of such size that the bulk of the wave energy is converted to energetic particle energy. The details of the process are fairly well accounted for in terms of a model which considers particles to be reflected from the walls of an expanding cavity produced by the radiation pressure. The larger the wave energy is, the wider the final vacuum cavity. Meanwhile, the propagating leading edge of the pulse imparts tremendous acceleration to both electrons and ions (positrons) in the direction of propagation through the Lorentz force. The acquired energy of these high-energy particles is proportional to the square of the wave amplitude, i.e., the wave intensity.

The organization of this paper is as follows. The simulation model is described in Sec. II. The particle acceleration mechanism and its effects are examined in Sec. III, while Sec. IV concentrates on vacuum formation and its effect on the wave spectra. Results obtained with a departure of the mass ratio from unity will be discussed in Sec. V. Finally, Sec. VI contains a discussion of the results.

II. THE MODEL

Simulation runs have been carried out on a relativistic electromagnetic code[10] with finite-size particles. The charged particles have a Gaussian distribution of charge in the x direction. They are allowed to have velocity components in the x, y, and z directions while all the physical quantities vary spatially only in the x direction. This is then a one- and two-halves-dimensional model. Fast Fourier transforms are used to calculate the field quantities from Maxwell's equations. The dipole expansion scheme is used to evaluate the plasma current and charge density associated with each grid point from the positions and velocities of the charged particles. The particle pushing is done according to the relativistic equations of motion. Standard space-time centering and leapfrog techniques are applied to solve the closed set of equations.

Particle momenta are advanced by an implicit matrix inversion. This matrix inversion imposes a stability condition for the code:

$$\Delta t < \frac{1}{2}\frac{\gamma mc}{eB}\ , \tag{1}$$

where Δt is the time step for orbit integration, γ is the relativistic factor for the electron, e and m are the charge and rest mass of the electron, and B is the wave magnetic field. In principle there can be particles whose velocity is small ($\gamma \sim 1$) which are located where the wave magnetic field B takes on a large value. This would indicate a small Δt would be required. However, such particles get accelerated forward in the x direction in practice and acquire a large total momentum and are expelled from the high-B field region. Moreover, as time elapses, the electromagnetic waves are trapped in a vacuum cavity. For these reasons, the physics of what happens does not seem to be affected by a fixed time step Δt throughout the run, although for some particles the condition, Eq. (1), was not satisfied at time $t = 0$. [This was tested by using different Δt's. At least in one case we chose Δt smaller than the value from Eq. (1) above for all the particles at $t = 0$, and obtained no appreciable difference from other runs].

A finite length train of electromagnetic radiation with wave number k_x is imposed on an initally uniform thermal electron-positron plasma with equal temperatures for both species. The direction of photon propagation, as well as of the allowed spatial variation, is taken to be the x direction. The system has typically the length $L_x = 1024\Delta$, Δ being the unit grid spacing taken equal to the electron Debye length λ_{De}, at $t = 0$. The speed of light is chosen to be $c = 5v_{te}$, where v_{te} is the electron thermal speed at $t = 0$; the photon wave number was taken to be $k_x = 2\pi/10\Delta$; the number of electrons and ions used was 10 240, i.e., 10 of each species per unit cell; and the size of the Gaussian-shaped particles was 1Δ.

To be strictly relativistic, the particle size should be Lorentz contracted as the particle becomes relativistic. A particle with no Lorentz contraction in the ultrarelativistic regimes has a highly expanded size compared with the size it should have. The use of finite-size particles alters the dispersion relation for wave propagation; the effect is simply obtained by replacing ω_p by $\omega_p e^{-k^2a^2/2}$ where a is the particle size. For a relativistic plasma we should use an average a^2, properly weighted by the Lorentz contraction. However, for the waves of importance in this simulation, the factor $e^{-k^2a^2/2}$ gives a correction of only 18% and would be smaller for contracted particles. The $\gamma^{-3/2}$ correction can be typically as large as 10^3 and appears to be the important relativistic correction. The frequency checks of a highly relativistic plasma from our simulation runs, however, show that the measured dispersion relations agree satisfactorily with the theoretical ones without finite particle size.

The relativistic character of the pulse is determined by the parameter $v_e = eE/m\omega c$ and $v_i = eE/M\omega c$ with M being the ion rest mass ($M = m$ for

positrons), ω the wave frequency, and E the wave amplitude at $t=0$. The parameter ν_e is varied from 1 to 20. The wave frequency is given as $\omega = (\omega_p^2 + k^2c^2)^{1/2}$, where ω_p represents the rest plasma frequency, i.e., $\omega_p = (\omega_{pe}^2 + \omega_{pi}^2)^{1/2} = \sqrt{2}\omega_{pe}$ for an electron-positron plasma. Underdense plasmas in the range $\omega \sim k_x c > \omega_p$ have been studied here. The length of the wave packet is chosen[2] to be $L_t \sim \pi c/\omega_{pe}$. For $k_x = 2\pi/10\Delta$, the wave packet length is 1.5 times the wavelength of the photon.

The initial linearly polarized pump wave has the form

$$E_y(x) = E \sin k_x(x - x_0), \tag{2}$$

$$B_z(x) = E\frac{k_x c}{\omega} \sin k_x(x - x_0) \sim E \sin k_x(x - x_0), \tag{3}$$

and the self-consistent momentum perturbation reads for each ith particle with charge e_i,

$$p_y(i) = p_t(i) + \mathrm{sgn}(e_i/e) p_w \cos k_x[x(i) - x_0], \tag{4}$$

for the interval $x = L_t = (50\Delta, 65.7\Delta)$ with $x_0 = 50\Delta$. The amplitude of the momentum modulation is given as $p_w = \nu mc$, and p_t is the thermal component of the initial momentum. With this assignment, the photon wave packet has a spectrum in k with a peak around $k = k_x$, and $\omega = (\omega_p^2 + k^2c^2)^{1/2}$, and propagates in the forward x direction at the photon group velocity, while approximately retaining its original polarization.

Periodic boundary conditions are used for the particles and field quantities. This has little effect on the interaction because the transit time of the particles and the waves across our long system in the preferential (forward) direction of propagation is longer than the saturation time when almost complete conversion of wave energy to particle kinetic energy is achieved. However, free space boundary conditions would help in absorbing the secondary backward propagating pulse associated with the lower edge of the vacuum which slightly perturbs the system upon reentry, as we shall see in the next sections.

III. PARTICLE ACCELERATION

A previous study using a similar setup,[2] but for an electron-ion plasma, has shown that a relativistic pulse creates a wake of plasmons whose electrostatic field in turn accelerates the electrons to extremely high energies. Tajima and Dawson[2] carried out simulation cases for $\nu \simeq 1$, since this is a region accessible to present day laser technology. This acceleration by the electrostatic plasmon field does not exist for an electron-positron plasma because the two charges respond equally to the ponderomotive force. Nonetheless, even in the absence of the above mechanisms, both electrons and ions are accelerated to very high energies in the direction of propagation by the relativistic pulse. We will first diagnose a run with $\nu_e = \nu_i = 5.8$, and then give a scaling law for the phenomena as ν is varied.

Acceleration of the particles by the pulse is clearly shown in Fig. 1 where a plot of the positron momentum in the x direction p_x versus the position x ("phase space") is shown. It is characterized by a thin streak of very large parallel momenta just ahead of the pulse, some reaching $p_x \sim 30mc$. A similar pattern holds for the electrons (Fig. 2), electrons and positrons move in unison longitudinally in the field of the pulse. Note the evacuated region in back of the streak. A comparison of the p_x phase space plot of Fig. 1 and the transverse electric field E_y of Fig. 3 (equivalent to a plot of B_z) indicates that the energetic streak follows the maximum amplitude part of E_y,

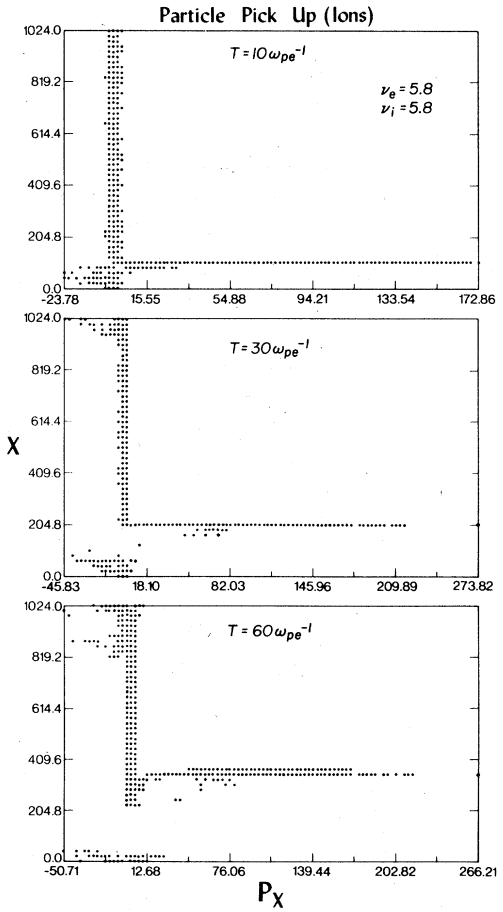

FIG. 1. Positron acceleration in the direction of pulse propagation. The xp_x phase space of the positrons is displayed, from top to bottom, at time $t = 10\omega_{pe}^{-1}$, $t = 30\omega_{pe}^{-1}$, and $t = 60\omega_{pe}^{-1}$, for $\nu_e = \nu_i = 5.8$. The momentum p_x is in units of mv_{te}, the position x in units of λ_{De}.

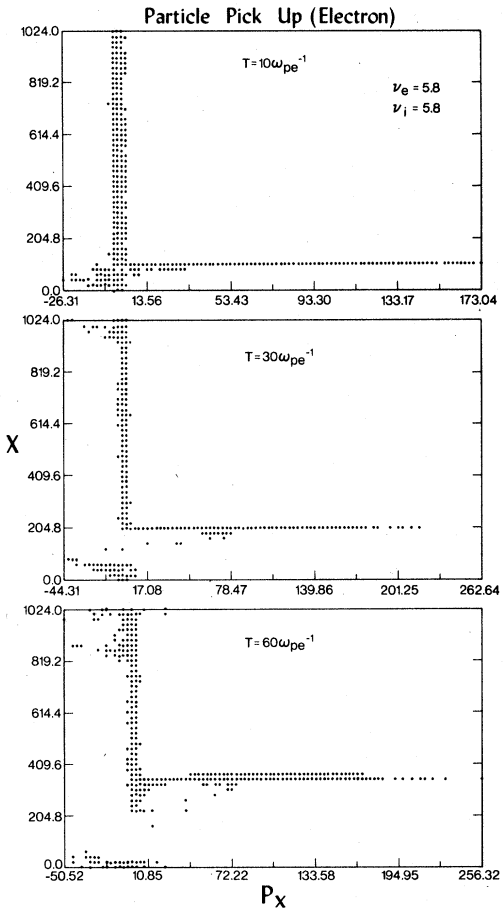

FIG. 2. Electron acceleration in the direction of pulse propagation. The xp_x phase space of the electrons is displayed at time $t=10\omega_{pe}^{-1}$, $t=30\omega_{pe}^{-1}$, and $t=60\omega_{pe}^{-1}$ for $\nu_e=\nu_i=5.8$.

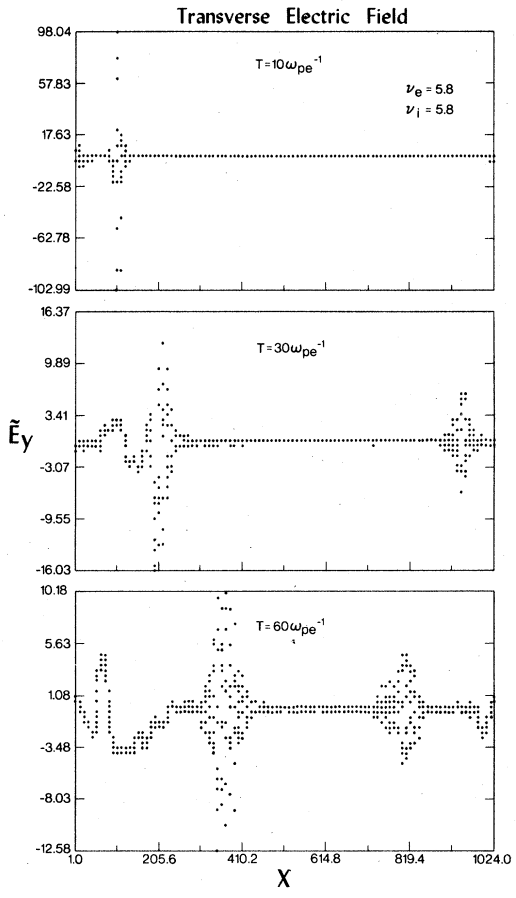

FIG. 3. Spatial variation of the transverse electric field E_y at $t=10\omega_{pe}^{-1}$, $t=30\omega_{pe}^{-1}$, and $t=60\omega_{pe}^{-1}$, for $\nu_e=\nu_i=5.8$.

set up by the initial perturbation, propagating according to $x\simeq x_0+ct$ in the positive x direction. Basically the forward acceleration is due to the $ev_y\times B_z/c$ force. In the ultrarelativistic regime, v_y is almost $+c$ where eE_y is positive and $-c$ where eE_y is negative. Then the y velocity is bent forward by the Lorentz force irrespective of the sign of the charge. At early times, however, the situation is slightly more complicated. Since p_y is 90° out of phase with B_z and E_y, there are particles which are accelerated backward in the x direction at early times. Then this motion through $v_x\times B_z$ tends to mitigate the E_y effect where E_y is negative [see Fig. 3(b)]. The transverse momentum p_y phase space is displayed in Fig. 4. One can pick out the particles moving with the pulse as a "straight line" following $x=x_0+ct$. The p_y phase space is, however, highly disturbed by the vacuum left behind by the pulse. The vacuum formation will be discussed in detail in Sec. IV.

It suffices to say here that from a comparison of Figs. 3 and 4, the maximum p_y is associated not with the main pulse but with the secondary one at the rear edge of the vacuum towards $x=0$. The backward propagating particles associated with the vacuum are responsible for the milder acceleration in the negative x direction behind the main pulse that shows up in Fig. 1. Throughout this development, the electrostatic field remains negligible. The sequence of events described above occurred for all values of ν tried.

An analysis of the runs for different values of ν reveals the following relationships. In all cases, the p_x momentum increases in time up to some saturation time t_s after which it oscillates about the value reached at t_s. This is accompanied by a corresponding decrease of the electromagnetic energy up to t_s, after which time it remains constant. The saturation time t_s is found to obey the following scaling:

$$t_s\propto\nu. \tag{5}$$

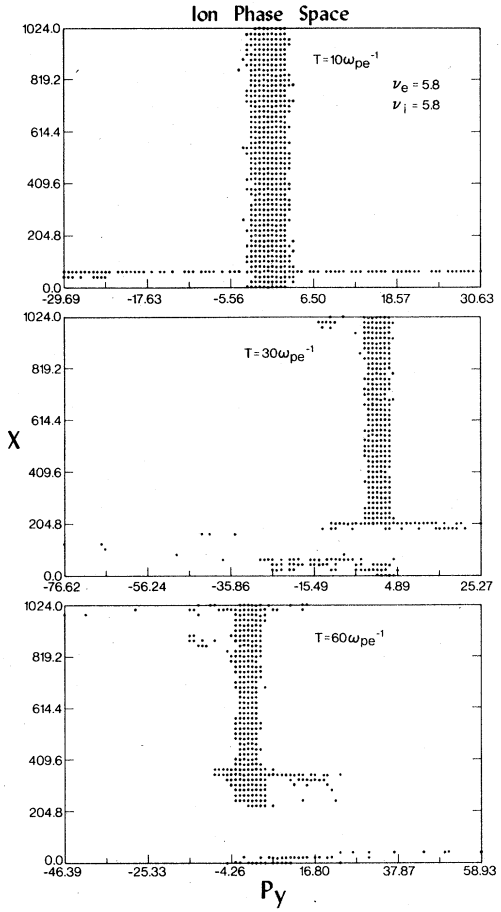

FIG. 4. The xp_y phase space of the positrons at $t = 10\omega_{pe}^{-1}$, $t = 30\omega_{pe}^{-1}$, and $t = 60\omega_{pe}^{-1}$ for $\nu_e = \nu_i = 5.8$.

It is linear with respect to ν with a coefficient $5\omega_{pe}^{-1}$ as shown in Fig. 5. This scaling is reasonable as we shall see later. Figure 6, where electron kinetic energy and electric-field energy are

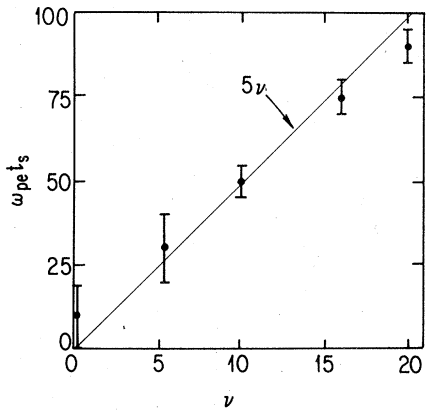

FIG. 5. Saturation time of the electron momentum and kinetic energy as a function of ν. Error bars are drawn in.

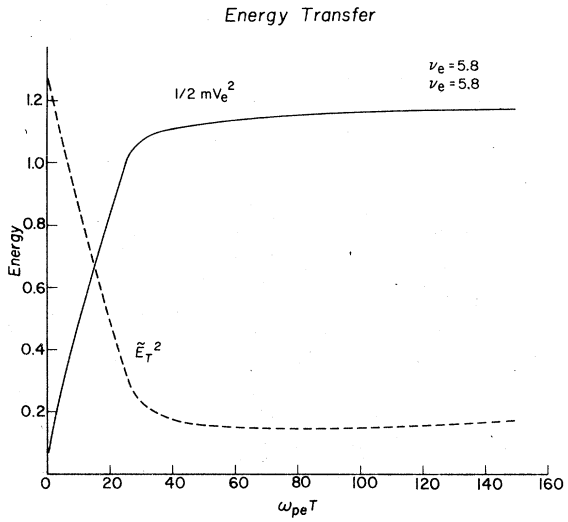

FIG. 6. Time evolution of the kinetic energy of the electrons and of the transverse electric energy of the electromagnetic wave.

plotted versus time for $\nu_e = \nu_i = 5.8$, illustrates that the energy transfer stops when the kinetic energy is equal to the initial wave energy. The time at which this happens is the momentum saturation time t_s. The change in kinetic energy is equal to the change in wave energy as required by energy conservation. The energies approximately follow the relationships

$$E^2(t) \propto e^{-t/\tau}, \tag{6}$$

$$\text{KE}\ (t) \propto (1 - e^{-t/\tau}). \tag{7}$$

The time constant τ is a linearly increasing function of ν as is t_s and $\tau \simeq t_s/2$. Similarly for all the values of ν tested, the maximum p_x momentum varies in time according to

$$p_x^m(t) \propto (1 - e^{-t/\tau}). \tag{8}$$

This is in agreement with the increase in kinetic energy $\sum_i [\gamma(i) - 1]mc^2$ where $\gamma(i)$ is the relativistic factor of each ith particle. Since $\gamma(i) \simeq p_x(i)/mc \gg 1$ and the particles that contribute the most are the energetic ones, the scaling of Eq. (8) is recovered from Eq. (7).

We have plotted in Fig. 7 the maximum p_x^m momentum in time, usually at $t = t_s$, versus the square of the wave relativistic factor ν^2. The maximum momentum increases linearly with ν^2 so that the following relationship holds:

$$p_x^m(t = t_s) \simeq \nu^2 mc. \tag{9}$$

The above scaling may be understood by a simple physical argument. The electromagnetic wave pressure acts as a piston on the relativistic electron-positron gas. In the frame moving with the interface, it is the particles that appear to do work

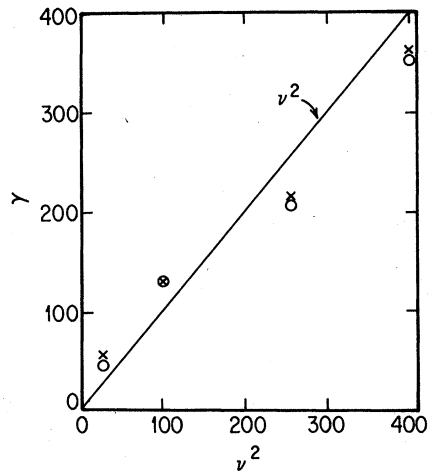

FIG. 7. Maximum particle relativistic factor ($\gamma \simeq p_x^m/mc$) in the direction of pulse propagation versus the square of the wave amplitude ν_e^2. The electrons are indicated by circles and the positrons by crosses. The full line follows ν_e^2.

on the piston, and pressure balance yields

$$2\langle n\rangle_w \langle p_x\rangle_w v_g = \tfrac{1}{2}[(E_w^2 + B_w^2)/8\pi], \tag{10}$$

where v_g is the piston (wave-front) velocity, the subscript w indicates that the fields, momentum, and density are to be evaluated in the moving frame of the interace, and $\langle n\rangle$ and $\langle p_x\rangle$ are, respectively, the average density and momentum at the leading edge of the pulse (over a length c/ω_{pe} in the laboratory frame). Lorentz transformations from the moving to the lab frame yield

$$2v_g(\langle n\rangle_L/\gamma_g)(\langle p_x\rangle_L/2\gamma_g) = \tfrac{1}{2}E_L^2/\gamma_g^2, \tag{11}$$

where the subscript L denotes laboratory frame variables and the relativistic factor $\gamma_g = [1-(v_g^2/c^2)]^{-1/2}$.

Our simulations show that $\langle p_x\rangle_L \simeq \frac{1}{2}p_x^m$ and $\langle n\rangle_L \simeq \frac{1}{2}n_{\max}$, with $n_{\max} \simeq 20n_0$ (twenty times the original density) at saturation, so that

$$p_x^m = 2(c/v_g)[\omega^2/\omega_{pe}^2(n_0)][\omega_{pe}^2(n_0)/\omega_{pe}^2(n_{\max})]\nu^2 mc. \tag{12}$$

With $\omega^2/\omega_{pe}^2(n_0) \simeq 10$ and $\omega_{pe}^2(n_0)/\omega_{pe}^2(n_{\max}) \simeq \frac{1}{20}$, we obtain

$$P_x^m \simeq (c/v_g)\nu^2 mc \sim \nu^2 mc, \tag{13}$$

in agreement with Eq. (8). An argument based on the fact that the final energetic particle energy equals the initial wave energy leads to the same scaling of p_x^m as ν^2.

The scaling law of the energy saturation time, Eq. (5), may be obtained by noting that $\dot{p}_x^m \simeq e\langle v_g B_z\rangle/c \simeq eB_z$. Integrating this equation in time, we obtain

$$P_x^m \lesssim et_s B_z(t=0) \simeq t_s \nu mc, \tag{14}$$

which gives rise, with the help of Eq. (13), to a scaling of

$$t_s \gtrsim \nu/\omega_{pe}. \tag{15}$$

We should remark that the number of very energetic particles at saturation is relatively independent of the wave amplitude ν. It is essentially the number of particles over the initial extent of the wave packet, here of the order of 1% of the total population for either species. These few energetic particles do, however, absorb most of the wave energy.

IV. VACUUM FORMATION

The strong forward exertion of light pressure causes a pile up of particles in front of the light pulse. This causes the plasma at the front to go overcritical to the wave, so that the wave does not penetrate the plasma. Also, since the expelled plasma is moving at close to c in the frame of the moving plasma, the wave is Doppler shifted to a frequency below cut off. The strong light pressure also ejects particles from where the pulse is located; the wave energy far exceeds the thermal energy of the plasma at $t=0$. As a consequence, the electromagnetic pulse is trapped in the vacuum cavity, while the pulse pressure continues to increase the volume of the vacuum, displacing the plasma particles forward at the leading edge of the pulse as well as backward at the tail of the pulse. The expansion of the volume (length) of the wave train L_t ends when most of the radiation energy is converted to particle energy.

This phenomenon can be seen in the p_x phase space of Fig. 8, again for $\nu_e = \nu_i = 5.8$. The vacuum size increases in time. Plots of the density (not shown) indicate a pile up of particles in a narrow region of space ($\sim c/\omega_{pe}$) slightly ahead of the pulse, a region at the original density well ahead of it, and a sizable vacuum behind. The appearance of a backward propagating pulse which eventually reenters the system at the upper x boundary is concurrent with the plowing of the particles by the pulse. There is also a large field perturbation associated with the *rear* edge of the vacuum which remains approximately at $x = x_0 = 50\Delta$. The maximum p_y perturbation accompanies this field structure.

The vacuum region exhibits the tendency to expand rapidly in time up to the point at $t = t_s$ when the maximum momentum is achieved; after this time the expansion rate decreases sharply. Then, the radiation pulse takes off on its own and propagates in the forward direction without altering the density further. For values of $\nu > 1$, the measured vacuum size expands in time according to

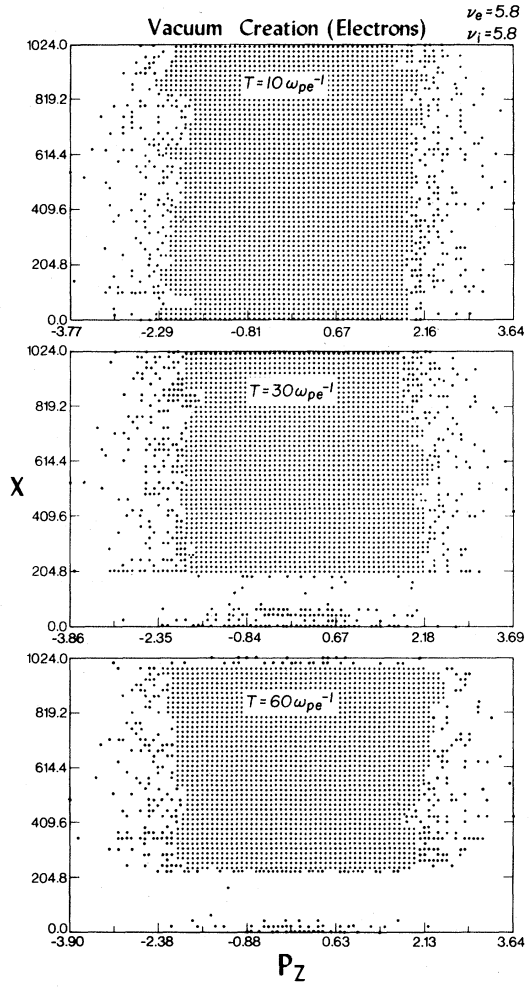

FIG. 8. An illustration of vacuum formation: The xp_z phase space of the electrons displayed, from top to bottom, at $t = 10\omega_{pe}^{-1}$, $t = 30\omega_{pe}^{-1}$, and $t = 60\omega_{pe}^{-1}$ for ν_e and $\nu_i = 5.8$.

$$L_v(t) = ct. \tag{16}$$

The vacuum length at the saturation time t_s is such that $L_v(t_s) = ct_s$. Figure 9 shows a linear depen dence of L_v as a function of ν. From Eq. (5), since $t_s \simeq 5\nu\omega_{pe}^{-1}$, we obtain

$$L_v(t_s) \simeq 5\nu c\omega_{pe}^{-1}, \tag{17}$$

in fair agreement with the increased lengths as shown in Fig. 9.

The presence of the vacuum is also reflected in the wave spectra. A time correlation of the electric field has been taken, integrated over the length of the run. The dispersion relation obtained from it is plotted in Fig. 10 again for $\nu_e = \nu_i = 5.8$, but the same pattern holds for other values of ν. For a light wave in a plasma, one would expect the frequency to follow $\omega^2 = \omega_p^2 + k_x^2c^2$ which is borne out by the two upper branches of

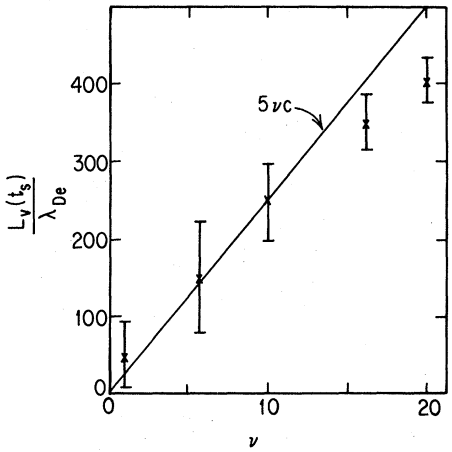

FIG. 9. Maximum vacuum length at saturation L_v normalized with respect to the Debye length λ_{De} as a function of the wave amplitude ν_e. The full line follows $5\nu_e c$ with c in units of v_{te}. Error bars are drawn in.

the simulation dispersion relation. Note the cut off at $\omega = \sqrt{2}\,\omega_{pe}$ for mode number = 0 or wave number $k_x = 0$. There appear, in addition to these normal plasma branches, two lower frequency branches which go like $\omega = k_x c$. Modes with $N = kL_x/2\pi > 6$ correspond to wavelengths such that $\lambda < L_v(t_s)$ and therefore fit in the vacuum region. For $N < 6$ the wavelength would be such that $\lambda > L_v(t_s)$. This suggests that the two lower branches are light waves which are trapped and propagating in the vacuum cavity. Light waves with $\lambda < L_v(t_s)$ should evanesce at the locations of high density.

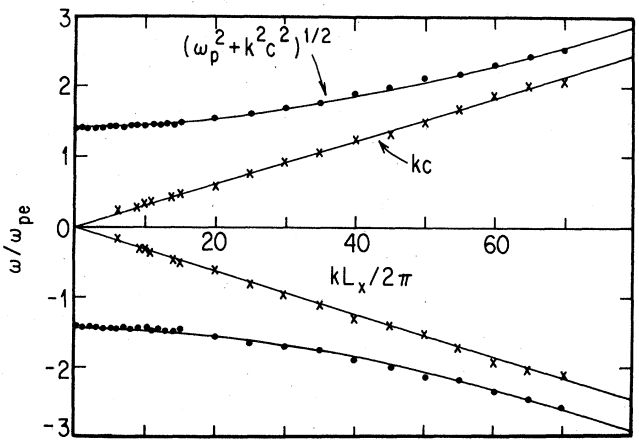

FIG. 10. The electromagnetic branch of the dispersion relation for $\nu_e = \nu_i = 5.8$. The frequency ω is plotted versus mode number. The upper and lower curves follow the plasma branch $\omega^2 = \omega_p^2 + k_x^2c^2$. The straight line follows the vacuum branch $\omega = \pm k_x c$. The measurable frequencies are plotted for all modes from 0 to 15 and every 5 modes thereafter.

We can rule out relativistic corrections to the light wave branch with frequency $\omega^2 = \omega_p^2/\gamma + k_x^2 c^2$ on the grounds that the most energetic particles, i.e., with $\gamma \gg 1$ only represent 1% of the total number of particles. Also, for most of the time over which the fields are correlated, the wave is below the relativistic limit it reached at the relatively short saturation time t_s compared to the overall correlation time. So far we have described cases of an electron-positron plasma, i.e., $M = m$. We will see in the next section how starting out with massive ions affects the results.

V. EFFECT OF ION INERTIA

Effects of ion inertia increase as the mass ratio M/m increases. Charge separation becomes more and more important as the ions lag the electrons in the longitudinal direction. Also the lower the v_e (down to $v_e \simeq 1$) and the greater the mass ratio, the more the situation of Tajima and Dawson[2] is approached, i.e., a wake of plasmons appears clearly for large mass ratios which accelerates electrons to high energies via electrostatic interaction. For high values of v_e ($v_e \gtrsim 5.8$), it is the Lorentz force, however, which dominates the acceleration process of both the electrons and ions in the direction of pulse propagation.

We concentrate here on cases where the value of v_e is fixed at $v_e = 20$ but the mass ratio is varied from 1 to 2 to 4 and finally to 10 so that v_i changed from 20 to 10 to 5 and finally to 2. The electrons are relatively unaffected by the change in the mass ratio. Their maximum forward momentum is of the same order of magnitude as M/m is varied; this is illustrated in Fig. 11, where the maximum relativistic factor of both electrons and ions ($\gamma \simeq p_x^m/m_0 c$, with m_0 either m or M) is plotted against the inverse of the mass ratio m/M. The saturation time of the electrons kinetic energy and momentum is independent of the mass ratio and remains at $t \simeq 90\omega_{pe}^{-1}$, i.e., the value of t_s obtained for $v_e = v_i = 20$.

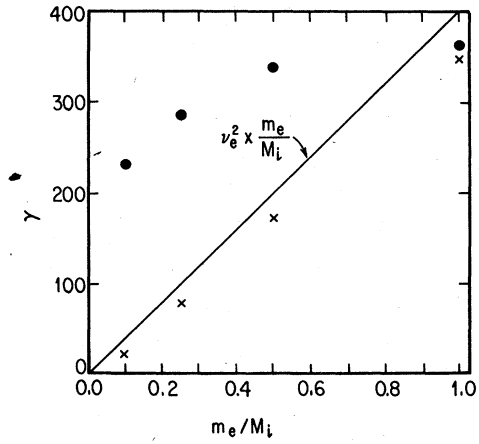

FIG. 11. Maximum relativistic factor ($\gamma \simeq p_x^m/mc$) for electrons and ions versus the inverse of the mass ratio m/M. The electrons are represented by circles and the ions by crosses. The full line follows $\gamma = (m/M)v_e^2$.

For the ions, on the other hand, as illustrated in Fig. 11, the maximum relativistic factor achieved ($\gamma_i \simeq p_x^m/Mc$) scales as

$$\gamma_i \simeq \gamma_e(m/M) \simeq v_e^2(m/M), \tag{18}$$

in other words, the maximum ion momentum achieved is independent of the mass ratio and approximately equal to that of the electrons. The electron and the ions end up with equivalent amounts of energy for larger γ or v from Eq. (18):

$$\mathrm{KE} \simeq \sum \gamma_i Mc^2 \simeq \sum \gamma_e mc^2, \tag{19}$$

where the sum is over all the particles of either species.

Saturation of the wave energy occurs when the ion kinetic energy equals the initial wave energy. The saturation time decreases as the mass ratio increases: $t_s \sim 90\omega_{pe}^{-1}$ for $M = m$, $65\omega_{pe}^{-1}$ for $M = 4m$, and $50\omega_{pe}^{-1}$ for $M = 10m$. At early times, the ions gain energy faster than the electrons. The strong electromagnetic waves eject the lighter electrons first, setting up a sizable ponderomotive force when the mass ratio is other than unity. The left-behind ions then get a large electrostatic acceleration as they catch up to the electrons, reach the relativistic regime, and overshoot in energy. The measured electrostatic force is in fact outward for the ions and inward for the electrons at the leading edge of the pulse. The region that became a vacuum for the equal masses case, now contains more particles that are not ejected by the wave as the mass ratio is increased. The extent of this vacuum or low-density region, however, is independent of the mass ratio and depends only on v_e.

The extent to which the ions will become relativistic in the pulse is inversely proportional to the mass ratio. The ions will remain nonrelativistic until $v_e > M/m$. In this limit of interest to pulsars, for example, the initial distinction between the rest masses will be insignificant.

VI. CONCLUSIONS AND DISCUSSION

An ultrarelativistic electromagnetic pulse ($eE/m\omega c \gg 1$) in an underdense plasma accelerates electrons and ions to high energies just ahead of the pulse in the wave propagation direction. As the wave becomes more relativistic, the difference between electron and ion inertia becomes

less significant and it may be expected that the plasma behaves like an electron-positron plasma. For marginally relativistic intensities ($eE/m\omega c \approx 1$) electrons are accelerated by an electrostatic plasma wave wake left behind the pulse; for the ultrarelativistic case in an electron-positron plasma particles are accelerated in the pulse propagation direction by the Lorentz force. This momentum conversion mechanism for acceleration is a very powerful one in the ultrarelativistic regime. As we increase the mass ratio from unity, charge separation and electrostatic acceleration of the ions become more pronounced. The maximum energies gained by ions and electrons remain constant irrespective of the mass ratio for a constant wave amplitude. When we vary the wave amplitude, the maximum energy particles gain is proportional to v_e^2 and the saturation time for energy increases as v_e. Simple physical arguments seem to be able to explain these scaling laws. The pulse leaves behind a very low density cavity or vacuum. The size of this region is again proportional to v_e. The electromagnetic waves become trapped in the cavity and give their energy to the particles through the radiation pressure acting on the walls of the expanding cavity. The trapped waves obey the vacuum dispersion relation $\omega = kc$.

Applications of these numerical simulations results to astrophysics are speculative. One scenario for pulsar evolution[11] suggests that relativistic plasma waves are a viable exterior magnetosphere for neutron stars below pair-production threshold.[12] Such waves are not expected for the observed pulsars, but may correspond to a much more numerous, as yet undiscovered, class of dead pulsars. Pulsars are known to occasionally adjust their rotation rate rapidly.[13] If such adjustments take place in less than a rotation period of a dead pulsar, a short radiation pulse might be emitted. The pulse might be observable from the radiation of its accelerated particles. Finally, extraordinarily intense brief pulses of electromagnetic, as well as gravitational waves, might be emitted during star collapse to a neutron star or black hole. The electromagnetic pulse should be rapidly converted to relativistic particles.

ACKNOWLEDGMENTS

The authors would like to thank J. Arons and F. Coroniti for fruitful discussions. This work was partially supported by National Science Foundation Contract Nos. PHY 79-01319 and ATM-78-19958, National Aeronautics and Space Administration Grant Nos. NSG/7341 and NAGW-78, and California Space Institute Grant No. CS79-9.

[1]See, for example, W. L. Kruer, in *Advances in Plasma Physics*, edited by A. Simon and W. B. Thompson (Wiley, New York, 1976), Vol. 6, p. 237.
[2]T. Tajima and J. M. Dawson, Phys. Rev. Lett. 43, 267 (1979).
[3]P. K. Kaw and J. M. Dawson, Phys. Fluids 13, 472 (1970).
[4]C. E. Max and F. W. Perkins, Phys. Rev. Lett. 27, 1342 (1971).
[5]C. F. Kennel, G. Schmidt, and T. Wilcox, Phys. Rev. Lett. 31, 1364 (1973).
[6]C. F. Kennel and R. Pellat, J. Plasma Phys. 15, 335 (1976).
[7]F. Pacini, Nature 216, 567 (1967); 219, 145 (1969).
[8]P. A. Sturrock, Astrophys. J. 164, 529 (1971).
[9]J. Hieronymus, Ph.D. thesis, Cornell University, 1971 (unpublished).
[10]A. B. Langdon and B. F. Lasinski, in *Methods of Computational Physics*, edited by B. Adler *et al.* (Academic, New York, 1976), Vol. 16, p. 327; A. T. Lin, J. M. Dawson, and H. Okuda, Phys. Fluids 17, 1995 (1974); T. Kwan, J. M. Dawson, and A. T. Lin, *ibid.* 20, 581 (1977).
[11]C. F. Kennel, F. S. Fujimura, and R. Pellat, Space Sci. Rev. 24, 407 (1979).
[12]M. Ruderman and P. G. Sutherland, Astrophys. J. 196, 51 (1975).
[13]M. Ruderman, Annu. Rev. Astron. Astrophys. 427 (1972).